2009 IEEE International Conference on Robotics and Automation
Kobe International Conference Center
Kobe, Japan, May 12-17, 2009

Piezoelectric Ultrasonic Resonant Micromotor with a Volume of Less Than 1 mm^3 for use in Medical Microbots

Brett Watson, James Friend, Leslie Yeo and Metin Sitti

Abstract— **To improve on current methods of minimally invasive surgery, research is being carried out on systems that will permit procedures to be conducted on the micro-scale using remotely operated micro-robots. One of the major stumbling blocks to meeting this need has been the absence of a practical micromotor with a volume of less than 1 mm^3 with which to drive these devices. To rectify this, we present a piezoelectric ultrasonic resonant micromotor with a volume of approximately 0.75 mm^3. The motor uses a novel helically cut stator that matches axial and torsional resonant frequencies, excited by a lead zirconate titanate element 0.03 mm^3 in volume. An earlier motor using the same stator design, but a larger overall volume, achieved a start-up torque of 47 nNm and no load angular velocity of 830 rad/s. This performance is on the order necessary to propel a swimming microbot in small human veins.**

I. INTRODUCTION

By 2050, the United Nations Department of Economic and Social Affairs Population Division reports that the number of older persons (>60 years) in the world will exceed the number of young persons (<15 years) for the first time in history [1]. Such an increase in the percentage of older persons will have a profound effect on the health care system. One method to help alleviate this is the increased use of minimally invasive surgery (MIS). MIS has been shown to decrease operation times and reduce hospital stays [2], alleviating some of the increased demand for hospital resources that comes with an ageing population.

To improve on current minimally invasive methods, research is being carried out on systems that will permit procedures to be conducted on the micro-scale in vivo, using remotely operated micro-robots (microbots). The ultimate aim of in vivo microbots is to carry out complex tasks including observation, sampling, drug delivery and performing surgical procedures within the cardiovascular, digestive and lymphatic systems. To facilitate the development of such devices, a practical micromotor with a volume of less than 1 mm^3 must be realised. These motors would be used not only to drive potential microbots, but also for the actuation of any tools that may be necessary to carry out the procedures (forceps, scalpel etc.).

Numerous designs have been proposed for small scale motors, the most successful of which include electrostatic [3], electromagnetic [4] and piezoelectric ultrasonic resonant [5] designs. By examining the physics of operation of the various motor designs, specifically the driving force used as the basis of design (electrostatic, electromagnetic and converse piezoelectric effect), it can be demonstrated that piezoelectric ultrasonic resonant motors have the largest potential for use as a practical micro-motor at sub-millimeter scales.

Despite having a large potential and despite some small scale piezoelectric ultrasonic resonant motors having been developed [5], [7], a practical sub-millimeter scale motor has not been achieved. We attribute this to a range of shortcomings that is common to current piezoelectric ultrasonic resonant designs. These include:

- Fragility – The stator of current designs is fabricated from a piezoelectric material. This makes the motors fragile to handle and potentially fragile during operation.
- Complex – Existing designs use multiple driving signals which lead to a complexity of control and the difficulty associated with multiple stator electrodes.
- Difficult to fabricate – The fabrication of small scale stators from a piezoelectric ceramic, with multiple electrodes is difficult, with the difficulty increasing as the scale decreases.

Through the use of a novel stator design that couples axial and torsional resonant frequencies, we have overcome many of these shortcomings. This has allowed us to take a significant step towards a practical motor with a volume of less than 1 mm^3.

II. BASIS OF OPERATION

Piezoelectric ultrasonic resonant motors make use of the converse piezoelectric effect. Specifically, a harmonic electrical input is applied to the piezoelectric element, which results in a harmonic strain in the direction of piezoelectric polarisation. With careful selection of electrical input frequency, the harmonic strain will excite a resonant mode (or modes) within the stator.

The goal of all stator designs is to effectively use the excited resonant modes to produce an elliptical motion at the stator tip (the point of contact between the stator and rotor, see Fig. 4). An elliptical stator tip motion is desirable as it results in the stator imparting both a contact (normal) and driving (tangential) force on the rotor, resulting in the rotor being driven by friction.

The method by which this achieved is known as the friction coupling. The principle of the friction coupling is to ensure that a larger contact force is exerted between the rotor and the stator for one half of the vibration cycle than the other half. Using a coulombic friction model, we can see

B. Watson, J. Friend and L.Yeo are with the Department of Mechanical and Aerospace Engineering, Monash University, Clayton, Vic, 3800, Australia james.friend@eng.monash.edu.au

M.Sitti is with the NanoRobotics Laboratory, Carnegie Mellon University, Forbes Avenue, Pittsburgh, PA 15213 USA

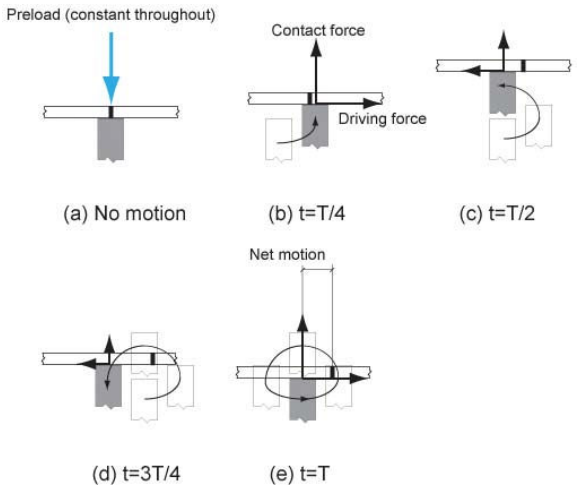

Fig. 1. By applying a "preload" to the rotor, it remains in contact with the stator for the complete cycle, ensuring a repeatable output. The elliptical motion provides a greater contact (and hence driving force) is applied during part of the cycle (b) and (e), than the other (c) and (d), resulting in a net motion.

that the cyclic contact force leads to a cyclic frictional force which, when time averaged across one stator cycle, results in a net work at the rotor in a given direction. This leads to a net motion of the rotor. We can see this illustrated in Fig. 1.

To ensure a constant contact force and repeatable rotor motion, a preload is used. This is a normal force on the rotor in the opposite direction to that imposed by the stator and is usually a magnetic, weight or spring force.

The most successful and popular designs to date use coupled orthogonal bending modes to elicit the elliptical motion at the stator tip [5], [7]. In general, the orthogonal modes are excited through the application of two electrical driving signals to a piezoelectric stator with multiple electrodes. Such designs carry the shortcomings described in Section I.

The design reported in this paper couples axial and torsional resonant modes of the stator. These modes are excited by a lead zirconate titanate (PZT) piezoelectric element external to the stator, which results in the desired elliptical stator tip motion. Fig. 2 demonstrates how the combination of the coupled mode shapes and the phase difference between the axial and torsional components, produces the desired elliptical motion at the stator tip. This methodology allows us to simplify the overall motor which has the following benefits:

- Less fragile – The proportion of piezoelectric ceramic used in the motor is greatly reduced, improving the robustness of the design. Also, the piezoelectric element is only used to excite a resonant mode, and does not operate at resonance itself. This improves the service life of the motor.
- Less complex – By coupling the axial and torsional resonant modes through the stator geometry, only one driving signal is required to run the motor.
- Easier to fabricate – The piezoelectric element is only a simple rectangular prism, making for easier fabrication. Other parts are fabricated by laser micro-machining, a method common in micro-stent and surgical implant fabrication.

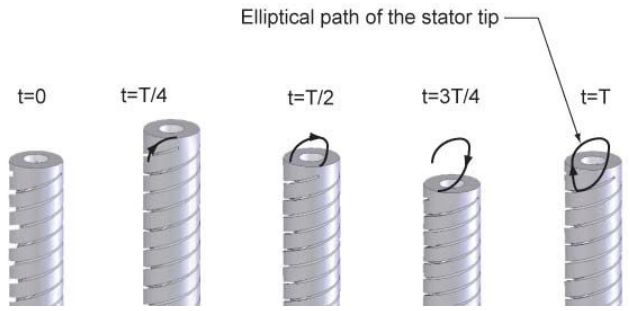

Fig. 2. The helical cuts in the stator allow the axial and torsional resonant modes to be coupled. This results in the desired elliptical stator tip motion as illustrated for one complete cycle. Note: t is time and T is period.

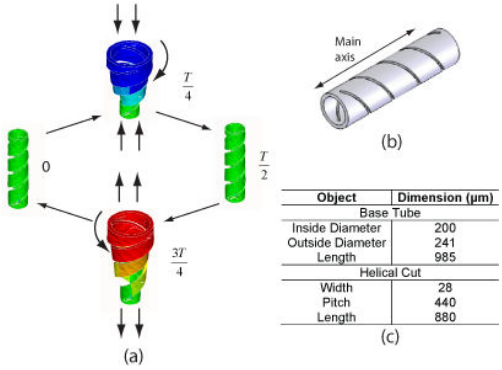

Object	Dimension (μm)
Base Tube	
Inside Diameter	200
Outside Diameter	241
Length	985
Helical Cut	
Width	28
Pitch	440
Length	880

Fig. 3. The (a) exaggerated ANSYS output confirming the motion of the stator during one cycle of period T as a consequence of the (b) helically-slotted tubular geometry of the stator. The (c) dimensions of the stator are on the order of hundreds of micrometers providing an overall stator volume of approximately 0.04 mm^3.

III. DESIGN AND TESTING

Based on the work by Wajchman et al. [9] an initial stator design using two helical revolutions (a helix angle of 30 °) was selected. The finite element analysis program ANSYS V10.0 (ANSYS Inc., Canonsburg, PA, USA) was used to conduct a limited parametric study on the proposed stator geometry, including cut width, cut length and number of cuts (helix starts). This study was used to determine a robust, geometric design and confirm the elliptical stator tip motion; the design however, is to be optimized at a later stage. Fig. 3 shows the resultant motion obtained through the selected stator design. The exaggerated ANSYS output highlights the coupling of the axial and torsional motion.

The fabricated design consists of a 304 stainless steel tube, with two diametrically opposite helical cuts removed (fabricated by Norman Noble Inc., Highland Heights, OH, USA), as detailed in Fig. 3. The piezoelectric element is a hard composition lead zirconate titanate (PZT) (C203, Fuji Ceramics, Tokyo, Japan), 3.5 mm in length, 2.5 mm in width, 0.27 mm in thickness, thickness poled, and was chosen due

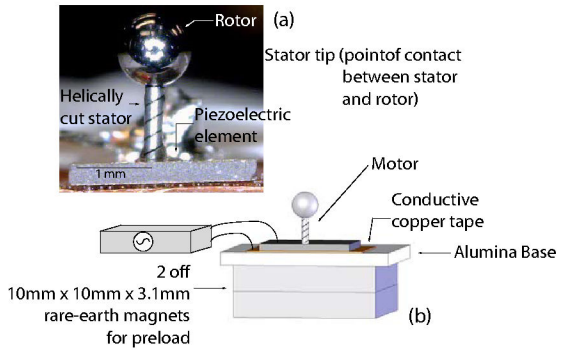

Fig. 4. A photograph of the motor (a), with a ∅241 m helically cut stator, ∅1 mm stainless steel ball (the rotor) and C203 PZT element. The motor is (b) connected to a signal generator, with copper tape atop an alumina base and magnets beneath to provide preload.

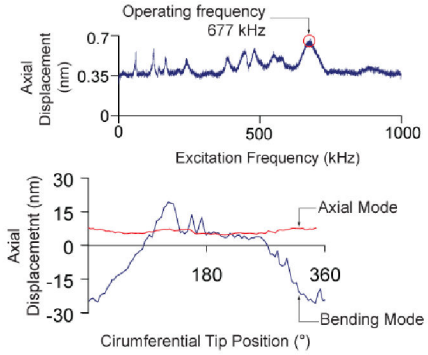

Fig. 5. Scanning LDV outputs including (a) the axial response spectrum for the stator tip that highlights resonant frequencies through spectral peaks and (b) the uniform stator tip profile of an axial mode (77 kHz, 19.3 V_{p-p}) and the varying profile of a bending mode (197 kHz, 20.3 $V_p - p$).

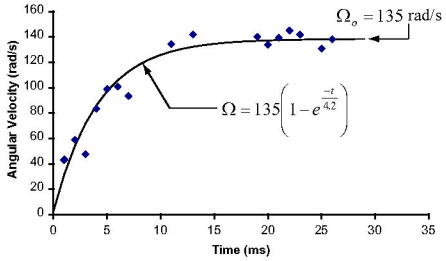

Fig. 6. Angular velocity vs. time results for an applied step voltage of 28.1 V_{p-p} and an operating frequency of 677 kHz. The fitted curve is derived using the method outlined in [11].

to availability. This was bonded by epoxy to one end of the helically cut stator to excite the stator's coupled resonant modes. A conductive copper tape was used to attach the PZT/stator component to an alumina base for testing.

Due to the small scale, a magnetic friction coupling was chosen. A stainless steel ball, 1 mm in diameter, served as a rotor, and was acted on by the magnetic preload. The arrangement of the motor components is shown in Fig. 4.

The axial response spectrum was recorded using a scanning laser doppler vibrometer (LDV) and associated software (MSA-400, Polytec GmbH, Waldbronn, Germany). The LDV measured the displacement of the stator tip in the direction of the stator's main axis (see Fig. 3) while simultaneously exciting all frequencies in the 0-1 MHz band. Peaks in the axial motion of the stator tip, are stator resonant frequencies. The axial spectrum is shown in Fig. 5. The mode at each resonant frequency was further analyzed using the scanning LDV to record the stator tip profile during one vibration cycle. Using the displacement profile, the resonant mode could be classified into an axial or bending based mode. As demonstrated in Fig. 5, an axial mode has an approximately uniform displacement across the tip. In comparison, a bending mode has a displacement change from positive to negative across the tip. Following the classification of modes, the motor was trialled at all modes that were axially based (axial/torsional coupled). Using a signal generator and amplifier (Rohde & Schwarz-SML 01 and NF-HSA 4501, North Ryde, NSW, Aust.), the PZT element was driven at each resonant frequency, and the performance was recorded.

Performance was determined using the method outlined by Nakamura et al. [11]. Rotor motion was recorded using a digital high speed camera (Olympus i-speed, Olympus Australia, Mount Waverley, Vic, Aust) at 1000 frames per second. The angular velocity vs. time data points were determined using the Olympus i-speed image processing software (V1.16, Olympus Industrial America, Orangeburg, NY, USA). The motor was found to have the highest start-up torque and rotational velocity when driven at the stator axial based resonance with the largest amplitude, 677 kHz. Applying a step input of 28.1 V_{p-p} as measured with an oscilloscope (LeCroy WaveJet 334, Chestnut Ridge, NY, USA), resulted in the angular velocity vs. time curve shown in Fig. 6. The fitted exponential curve is derived from the standard curve for a piezoelectric ultrasonic motor [11].

The no load angular velocity recorded for the motor was 135 rad/s (1295 rpm). Using this as an input for the method outlined in [11] the maximum start-up torque, based on the curve shown in Fig 6, was calculated to be 13 nNm. For the chosen operating mode, the motor had an operating frequency range of 652–682 kHz. The performance of this prototype compares well with other piezoelectric ultrasonic micro-motors, with 52% of the torque achieved at 32% of the size of the most comparably sized stator [5].

IV. IMPROVED PERFORMANCE THROUGH MORE STRONGLY COUPLED RESONANT MODES

From the initial study we can see that a motor design that couples axial and torsional resonant modes achieves a similar performance to existing motor designs, but at a smaller scale. However, during the analysis it was found that the axial and torsional modes of the initial design were only weakly coupled, with the axial resonant frequency approximately 30% higher than the equivalent torsional harmonic. This

arose from the initial design being based on a "twisted beam" structure. We hypothesise that a design that more strongly matches the axial and torsional modes would improve motor performance.

To achieve such a design, we carried out a finite element parametric study using ANSYS V10.0 (ANSYS Inc., Canonsburg, PA, USA). The aim of the study was to determine the set of stator geometric parameters required to strongly couple the axial and torsional resonant modes. The parameters examined were:

- Stator Length (L_z)
- Ratio of internal to external diameter ($\frac{D_i}{D_o}$)
- Cut width (CW)
- Number of cuts (N_c)
- Number of helix turns (helix pitch) (N_r)

Internal and external diameter of the stator were fixed at the values of a 32-gauge tube (smallest commercially available tube). Material density (ρ) was kept constant for stainless steel.

By using a modifed version of Wittrick's spring stiffness model [18] we were able to reduce the parameters to only include the stator length (L_z) and the stator's equivalent axial (K_e) or torsional (K_r) spring stiffness. Using Buckingham's Pi theorem we were then able to collapse the data using equation 1. The collapsed data is shown in Fig. 7.

$$Log(\frac{F_x}{n}) = \frac{1}{2}Log(\frac{K_x}{\rho}) - \frac{3}{2}Log(L_z) \qquad (1)$$

where F is the resonant frequency, n is the harmonic number associated with the resonant frequency and $x = e$ (axial) or $x = r$ (torsional). We refer to the left-hand side of the equation as the "Non-dimensional resonant frequency" and the right hand side of the equation as the "Non-dimensional geometric parameter".

From the study we found it was possible to obtain a multiple sets of geometric parameters that match the axial and torsional resonant frequencies. We also noted that the number of helix turns and number of helical cuts being the most important parameters in achieving this.

To validate the ANSYS model and confirm the study results, a modified version of the method outlined by Friend at al. [12] was used. This method compares LDV measured displacement spectra at six points on the stator tip. With sensible application, this method allows the mode to be classified directly from these spectra. Fig. 8 shows the recorded spectra and comparable ANSYS results for a stator with five helix rotations and two cuts.

From the study, a stator geometry using 3.5 helix revolutions and three identical helical cuts was chosen. Geometry dimensions are detailed in Fig. 9. The revised prototype was fabricated from a 304 stainless steel tube with the helical cuts laser cut at equal circumferential spacing (Laser Micromachining Solutions, Macquarie University, NSW, Aust.). The magnetic preload was increased through the use of an

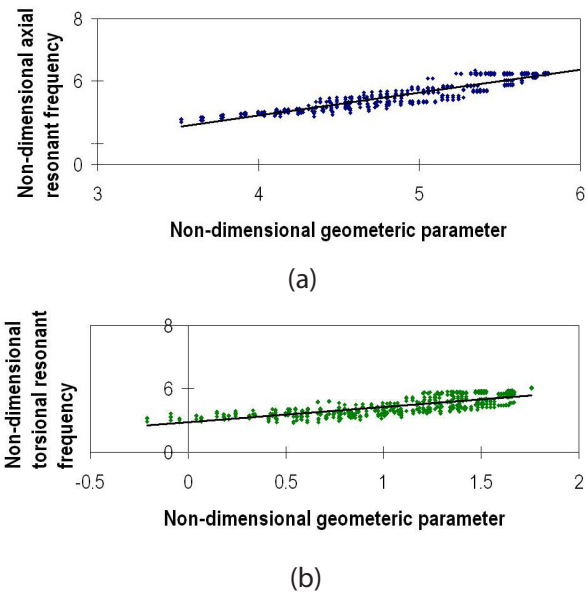

Fig. 7. Finite element analysis was used to determine the axial and torsional resonant frequencies of the stator whilst varying the geometric design parameters. These results were then collapsed using Buckingham's Pi Theorem (equation 1) to give the non-dimensionalised axial (a) and torsional (b) results shown here.

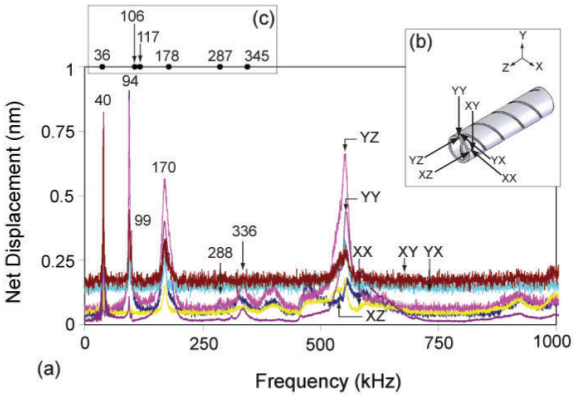

Fig. 8. Comparison of stator resonant frequencies obtained from (a) LDV recorded displacement spectra, using the measurement positions detailed in (b), and (c) ANSYS calculated frequencies for a stator with five helix revolutions and two helical cuts.

additional NdFeB magnet, 0.4 mm in diameter and 1 mm in length. This was necessary to cope with the increase in performance of the revised design. All other aspects of the set up were the same as for the motor described in Section III.

The motor was trialled for each of the finite element model derived axial/torsional coupled resonant frequencies using a bandwidth of $\pm 5\%$ to allow for manufacturing tolerances. The motor demonstrated bi-directional operation with clockwise rotation at the third harmonic, 732 kHz and counterclockwise rotation at the second harmonic, 526 kHz. As in Section III motor performance was determined using the method by Nakamura et al. [11]. Rotor motion was recorded using a laser doppler velocimeter (Cannon LV-20Z, Kiyohara-Kogyodanchi, Utsunomiya-shi, Tochigi-ken,

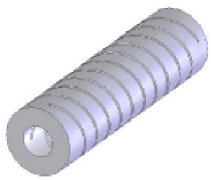

Object	Dimension (μm)
Base Tube	
Inside Diameter	200
Outside Diameter	241
Length	985
Helical Cut	
Width	28
Pitch	440
Length	880

Fig. 9. Revision of the stator geometry following further analysis allowed the axial and torsional resonant frequencies to be more closely matched.

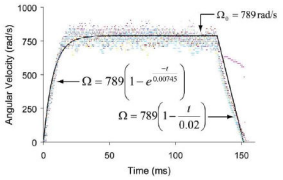

Fig. 10. Angular velocity vs. time results for an applied step voltage of 20 V_{p-p} and an operating frequency of 732 kHz. The fitted curve is derived from the method in [11] and is the average obtained across all runs.

Japan). A maximum clockwise angular velocity of 830 rad/s (7,925 rpm) was recorded at an input of 20 V_{p-p} and 732 kHz. Based on the curve in Fig. 10, the average clockwise start-up torque was 47 nNm with a peak of 51 nNm and a minimum of 39.8 nNm. The average breaking torque was calculated to be 17.8 nNm. A maximum counterclockwise angular velocity of 1600 rad/s (15,280 rpm) at 32.1 V_{p-p} and 526 kHz was recorded; however, the inconsistent nature of the operation prevented the measurement of the complete motor performance.

V. SMALL SCALE MOTOR

The most recent motor set up makes use of this increased performance to produce a design with a volume of approximately 0.75 mm^3. It must be noted that this volume excludes the second large rare earth magnet used for the preload.

In this design, the original piezoelectric element is replaced with a PZT element with dimensions 250 μm x 250 μm x 500 μm. Epotek H20E (Elecsys LLC, Procidence, RI, USA) silver conducting epoxy is used to provide the connections between the PZT element and electrical wiring and PCB mounting board. Fig. 11 shows the experimental setup. The motor was operated in the clockwise and counterclockwise directions.

VI. DISCUSSION

By using a stator geometry that more strongly couples the axial and torsional resonant modes, the motor performance was substantially improved. Angular velocity has been improved by a minimum of 5.5 times across all runs, with the start-up torque increased by a minimum of 3 times. A proportion of this improvement can be attributed to the increased preload; however, the increase in preload is considered to be substantially less than the improvement in performance.

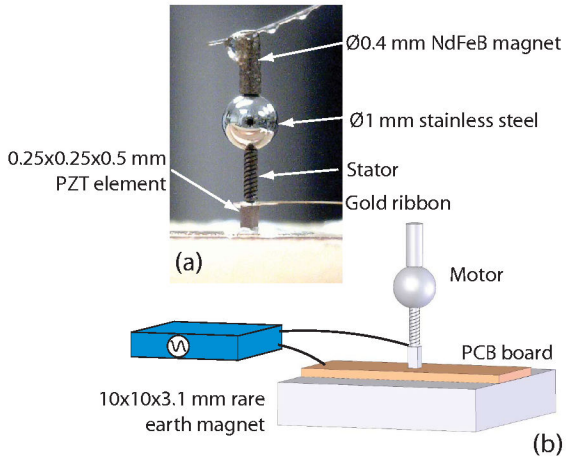

Fig. 11. A photograph of the motor (a), that uses a small lead zirconate titanate (PZT) element, reducing the motor volume to approximately 0.75 mm^3. The motor is (b) connected to a signal generator, using gold ribbon and a PCB board with silver conducting epoxy connection.

The revised stator geometry also demonstrated bi-directional operation, an improvement over the initial tested design. Counterclockwise operation however, was unreliable when compared with clockwise operation. This can be attributed to the increased angular displacement achieved during each cycle in the clockwise direction due to the stator's tendency to uncurl in that direction during axial displacement. This same tendency will hinder motion in the counterclockwise direction. By ensuring future motors match the PZT thickness resonance with the operating frequencies, this will be less pronounced, enabling reliable bi-directional operation to be achieved.

The motor design has been demonstrated to work using a micro-scale piezoelectric element. It is not expected that this new design will lose performance over the older, larger designs due to the increase in the thickness of the piezoelectric element. This will allow the stator and PZT resonance modes to be more easily matched and enable the use of higher input voltages. However, to complete the design a revised friction coupling not using a large magnetic element must be arrived upon.

To give an example of the potential application for such a motor, we examine a "swimming microbot" that uses an E.coli like flagella as a means of propulsion. Such microbots have been highlighted as having a great potential for use in in vivo medical procedures due to the low Reynolds number propulsion system [13]. These robots are prime candidates for the next generation of MIS discussed in Section I. The flagellum would be attached directly to the rotor of the piezoelectric motor discussed in this paper. A concept design is illustrated in Fig. 12.

Using Higdon's model for flagellar propulsion [14], we may determine the average power required for swimming in small human arteries from:

$$\bar{P} = 6\pi\mu A\bar{U}^2\eta_0^{-1}K$$

where blood has a viscosity of approximately μ =0.0035 Pa-

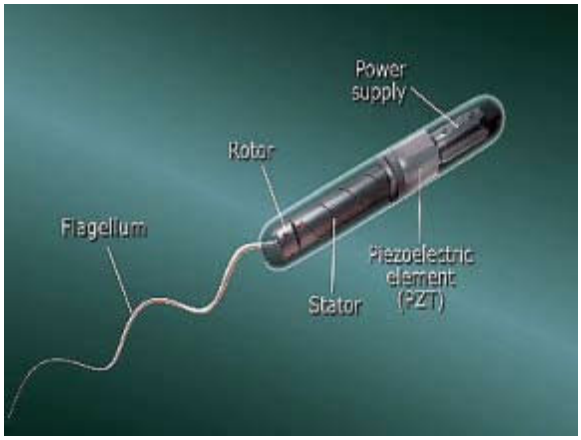

Fig. 12. A concept design of a "swimming microbot" using the piezoelectric ultrasonic resonant micromotor.

s [15], A, is the radius of the swimming microbot which we'll assume to be approximately the size of the motor – 150 μm, K is the Stoke's law correction for a prolate spheroid – 2.7 [16], leaving only the swimming speed $\bar{U}$ to be defined, if we take Higdon's results and set $\eta_0^{-1} = 200$. If we assume the device should swim at a nominal velocity of 2 cm/s against the blood flow, and consider a vein in the eye as a suitable example of a location both difficult to reach by other means and presumably one where this device would be used, $\bar{U} \approx 2 + 1.9$ cm/s [17], giving a required input power of 8.1 μW.

The average power output of the motor is approximately $(\phi_{max} T_{max})/4 = 9.75$ μW, where ϕ_{max} is the maximum clockwise velocity and T_{max} is the average start-up torque. As can be seen, this is in excess of what is required in the above example.

VII. CONCLUSION

We have demonstrated a motor with a volume of less than 1 mm^3. This was achieved through the use of a novel stator design that coupled axial and torsional resonant modes, simplifying current piezoelectric ultrasonic resonant designs and making use of the thus far unfulfilled potential of this class of motors. Motor performance was shown to increase greatly by ensuring the fundamental axial and torsional resonant modes were strongly coupled through careful geometric design. This level of performance was demonstrated to be enough to theoretically propel a swimming microbot in the human body. A continued improvement in this motor may lead to the advances in minimally invasive surgery necessary to help overcome the strains that will be placed on the health care systems of the world as the population continues to age.

VIII. ACKNOWLEDGMENTS

This work was made possible in part by grants SM/07/1616 and SM/06/1208 from the CASS Foundation, grant DP0773221 from the Australian Research Council, and the New Staff and Small Grant Scheme funds from Monash University. "This work was performed in part at the Macquarie/ATP node of the Australian National Fabrication Facility. A company established under the National Collaborative Research Infrastructure Strategy to provide nano and microfabrication facilities for Australia's researchers. [sic]"

REFERENCES

[1] United Nations Department of Economic and Social Affairs Population Division,"World Population Ageing: 1950-2050", *2002 World Assembly on Ageing*, 2002

[2] N.T. Nguyen and D.M. Follette and B.M. Wolfe and P.D. Schneider and P. Roberts and J.E. Goodnight Jr, Comparison of Minimally Invasive Esophagectomy With Transthoracic and Transhiatal Esophagectomy, *Archives of Surgery*, vol. 135, 2000, pp 920-925.

[3] M. Mehregany and P. Nagarkar and S.D. Senturia and J.H. Lang, Operation of Microfabricated Harmonic and Ordinary Side-Drive Motors, *Proceedings of the IEEE Micro-Electro-Mechanical Systems Workshop*, 1990, pp 1-8

[4] K. Hori and T. Miyagawa and L.Ito, Development of Ultra-Small Sized Servo Actuator with Brushless DC Motor, Planetary Gear Drive and Optical Rotary Encoder, *International Journal of the Japan Society for Precision Engineering*, vol. 31, 1997, pp 1-5

[5] T. Kanda and A. Makino and L. Suzumori and T. Morita and M.K. Kurosawa, A Cylindrical Micro Ultrasonic Motor using a Micromachined Bulk Piezoelectric Transducer, *IEEE Ultrasonics Symposium*, 2004

[6] Z.L. Wang, Nanopiezotronics, *Advanced Materials*, vol. 19, 2007, pp 889-892

[7] H. Zhang and S. Dong and S. Zhang and T. Wang and Z. Zhang and L. Fan, Ultrasonic Micro-motor using Miniature Piezoelectric Tube with Diameter of 1.0 mm, *Ultrasonics*, vol. 44, 2006, pp e603-e606

[8] K. Uchino, Piezoelectric Ultrasonic Motors: Overview, *Smart Material Structures*, vol. 7, 1998, pp 273-285

[9] D. Wajchman and D. Liu and J. Friend and L. Yeo, An Ultrasonic Piezoelectric Motor Utilising a Non-Circular Cross Sectioned Twisted Beam, *IEEE Transactions on Ultrasonics, Ferroelectrics and Frequency Control*, 2008, vol. 55, 2008, pp 832-840

[10] J. Tsujino, Ultrasonic Motor Using a One-Dimensional Longitudinal-Torsional Vibration Converter with Diagonal Slits, *Smart Material Structures*, vol. 7, 1998, pp 345-351

[11] K. Nakamura and M.Kurosawa and H. Kurebayashi and S.Ueha, An Estimation of Load Characteristics of an Ultrasonic Motor by Measuring Transient Responses, *IEEE Transactions on Ultrasonics, Ferroelectrics and Frequency Control*, vol. 38, 1991, pp 481-485

[12] J. Friend and K. Nakamura and S. Ueha, A Torsional Transducer through In-Plane Shearing of Paired Planar Piezoelectric Elements, *IEEE Transactions on Ultrasonics, Ferroelectrics, and Frequency Control*, vol. 51, 2004, pp 870-877

[13] B. Behkam and M. Sitti, Design Methodology for Biomimetic Propulsion of Miniature Swimming Robots, *ASME Journal of Dynamic Systems and Measurement Control*, vol. 128, pp 36-43

[14] J.J.L. Higdon, The Hydrodynamics of Flagellar Propulsion: Helical Waves, *Journal of Fluid Mechanics*, vol. 94, 1978, pp 331-351

[15] P.W. Rand and E. Lacombe and H.E. Hunt and W.H. Austin, Viscosity of normal human blood under normothermic and hypothermic conditions, *Journal of Applied Physiology*, vol. 19, 1964, pp 117-122

[16] J. Happel, H.Brenner, *Low Reynolds Number Hydrodynamics*, Prentice Hall, Englewood Cliffs, NJ; 1965

[17] T. Tanaka, C. Riva, I. Ben-Sira, Blood Velocity Measurements in Human Retinal Vessels, *Science*, vol. 186(4166), 1974, pp 830-831.

[18] W.H. Wittrick, On Elastic Wave Propagation in Helical Springs, *International Journal of Mechanical Sciences*, vol. 8, 1966, pp 25-47